Author: H. Jelinek, M. Cree, J. Leandro, J. Soares, R. M. Cesar and A. Luckie
Author Address: hjelinek@csu.edu.au
m.cree@waikato.ac.nz
Title: Automated segmentation of retinal blood vessels and identification of proliferative diabetic retinopathy
Year: 2007
Journal: Journal of Optical Society of America, A.
Volume: 24
Issue: May
Pages: 1448-1456
ISSN: 1084-7529
DOI: URL: http://dx.doi.org/10.1364/JOSAA.24.001448
Abstract Proliferative diabetic retinopathy can lead to blindness. However early recognition allows appropriate, timely intervention. Fluorescein-labelled retinal blood vessels of twenty-seven digital images were automatically segmented using the Gabor wavelet transform and classified using traditional features such as area, perimeter and an additional five morphological features based on the derivatives-of-Gaussian wavelet derived data. Discriminant analysis indicated that traditional features do not detect early proliferative retinopathy. The best single feature for discrimination was the wavelet curvature with an area under the curve (AUC) of 0.76. Linear discriminant analysis with a selection of six features achieved an AUC of 0.90 (0.73–0.97 95% CI). The wavelet method was able to segment retinal blood vessels and classify the images into proliferative retinopathy present or absent.

Automated segmentation of retinal blood vessels and identification of proliferative diabetic retinopathy

Herbert F. Jelinek

School of Community Health, Charles Sturt University, Wilson St. Albury 2640, Australia.

Michael J. Cree

Department of Engineering, University of Waikato, Hillcrest Rd., Hamilton 3240, New Zealand.

Jorge J.G. Leandro

Creative Vision Research Group, Department of Computer Science, IME – University of São Paulo, Brazil.

João V.B. Soares

Creative Vision Research Group, Department of Computer Science, IME – University of São Paulo, Brazil.

Roberto M. Cesar-Jr.

Creative Vision Research Group, Department of Computer Science, IME – University of São Paulo, Brazil.

A. Luckie[4]

[4]Albury Eye Clinic, Swift St. Albury 2640, Australia.

Proliferative diabetic retinopathy can lead to blindness. However early recognition allows appropriate, timely intervention. Fluorescein-labelled retinal blood vessels of

twenty-seven digital images were automatically segmented using the Gabor wavelet transform and classified using traditional features such as area, perimeter and an additional five morphological features based on the derivatives-of-Gaussian wavelet derived data. Discriminant analysis indicated that traditional features do not detect early proliferative retinopathy. The best single feature for discrimination was the wavelet curvature with an area under the curve (AUC) of 0.76. Linear discriminant analysis with a selection of six features achieved an AUC of 0.90 (0.73–0.97 95% CI). The wavelet method was able to segment retinal blood vessels and classify the images into proliferative retinopathy present or absent.

100.5010 Pattern recognition and feature extraction

Introduction

Diabetes and its associated complications, including diabetic retinopathy (DR), has been identified as a significant growing global public health problem.[1] Between 22% - 36% of people with diabetes have retinopathy and of those one-third have vision threatening retinopathy.[2] Those with retinopathy will lose vision leading to potential blindness and loss of quality of life if not treated.[3] In proliferative retinopathy new blood vessels are formed that emerge from the area of the optic disk and spread towards the macula or emerge from peripheral vessels.[4] Timely intervention for diabetic retinopathy lessens the possibility of blindness.[5, 6]

Retinal Blood Vessel Segmentation

A necessary initial step in applying shape analysis to retinal blood vessels is to segment the blood vessels from the background.[7] Segmentation algorithms for retinal blood vessels are numerous and have been described in detail elsewhere. Different approaches have

explored image processing techniques such as matched filters, mathematical morphology, threshold probing, supervised classification, deformable models, and tracking.[8-14] We have developed a supervised approach for vessel segmentation based on the continuous wavelet transform (CWT), which has shown to outperform other state-of-the-art methods with respect to ROC analysis on public retinal image databases.[15-17] This segmentation approach is applied in the present paper for the detection of proliferative retinopathy using fluorescein labelled images of the posterior pole. There is no difference in principle between using fluorescein labelled images versus images obtained using a colour non mydriatic camera as the segmentation algorithm is applied to the green channel only. The CWT is a powerful and versatile tool that has been applied in many different image processing problems, from image coding to shape analysis.[18] This success is largely due to the fact that wavelets are especially suitable for detecting edges in signals such as blood vessel borders and performing fractal and multifractal analysis.[19-21] Fluorescein angiograms generally require parameter reconfiguration for most methods in the literature. One of the advantages of our approach is that it aims at minimizing the need for reconfiguring the automated segmentation parameters for every fluorescein image by applying a supervised classification procedure which only depends on manually segmented images to compose a training set for segmentation.

Classification of proliferative diabetic retinopathy

Research into automated assessment of optic fundus images has mainly concentrated on the identification of features associated with non-proliferative diabetic retinopathy.[22-25]. Interpreting changes in the branching pattern of retinal blood vessels remains a challenge in assessment of proliferative diabetic retinopathy (PDR). As there is no a priori way of identifying appropriate shape features for studying pathological changes in retinal blood

vessels, the task remains to search for new shape features that add new explanatory power and diagnostic accuracy. Vessel morphology has been quantified with geometrical/metric and topological parameters such as length, angles, branching order, tree asymmetry, bending energy, fractal dimension, Sholl diagrams and area of influence.[8, 26-28] Early studies concentrated on the analysis of optic fundus blood vessel patterns using hand-drawn vessel patterns to analyse morphological features. These studies demonstrated that vessel occlusion and neovascularisation could be identified using a feature parameter such as fractal analysis.[28] The Gabor wavelet used here to segment the blood vessels is very efficient through its wavelet characteristics, reducing overall computation time. The resulting vessel patterns are then characterised by several feature parameters based on the wavelet derived information.

In the present paper we explore our previously described method for the segmentation of the retinal blood vessels.[17] We then show that the wavelet approach may also be successfully used for describing structural attributes possibly associated with proliferative diabetic retinopathy. As PDR is defined by a change in vessel pattern by either loss or addition of vessels within the retina, a skeletonised vessel pattern is sufficient for classification.

The shape features adopted here are based on calculating wavelet gradients from skeleton images followed by the extraction of meaningful measures including 2nd wavelet moment, entropy of orientation, curvature and fractal dimension. Such wavelet shape features have already been successfully employed for the characterization of another type of branching structure, i.e. neural cells.[29] Hence, the results reported here show that the wavelet approach is suitable for both segmentation and morphological characterization of retinal blood vessels in the context of proliferative retinopathy. Proliferative diabetic retinopathy is

characterised early by the presence of ischaemic areas, where a loss of blood vessels occurs and later by newblood vessel formation caused by several angiogenic factors. Thus the blood vessel pattern obtained using the Gabor wavelet for retinae with PDR should be distinctly different to those retinae without PDR.

Methods

Vessel segmentation

Image acquisition

Twenty-seven images (1024x1024 pixel) were obtained using a Topcon camera linked with Image 2000 software. Of these sixteen were of proliferative retinopathy and the remaining eleven without but with background retinopathy and other pathology. These images were exported as TIFF images using the Object-Image imaging software (http://rsb.info.nih.gov/nih-image/). The vasculatures were then manually traced and automatically segmented for further analysis.

Wavelet transform for vessel segmentation

The wavelet transform is used for two important different purposes in the context of the present paper: vessel segmentation and morphological characterisation. Firstly, we applied the Gabor wavelet transform, which differentiates the blood vessels from the background in conjunction with a training set based on the manually traced training images. The complete process has been described elsewhere and is summarised here.[17, 27]

The property of being well localised both in the time and frequency domain makes wavelets adequate for local filtering and allows detection of localised singularities, such as blood vessels.[30] The Gabor wavelet was superimposed onto each pixel of the image at various angles and scales. In order to detect the blood vessels, for each scale value chosen, the

transform was calculated over the range of 0 to 170 degrees, at steps of 10 degrees, and the feature space was updated with the maximum value at each pixel position. Thus, the features used to identify vessel pixels were the maximum transform responses over all angles for different scale values (to span all possible vessel widths) and also the original pixel intensity value. The wavelet parameters associated with the Gabor wavelet (scale, frequency, elongation) were empirically determined in order to reach the best matching between wavelet and vessels. Once determined, the parameter configuration did not have to be changed from image to image and represented the final feature space for vessel segmentation.[31]

A normal transformation was applied to all features to obtain dimensionless values, which allows a comparison between features and avoids mistakes in classification steps, since different units would affect the distance in the feature space.[18] The normal transformation is defined as

$$\hat{v}_i = \frac{v_i - \mu_i}{\sigma_i}$$

where $\hat{v}_i$ is the *i*-th transformed feature, v_i is the *i*-th original feature, μ_i is the average value of the *i*-th feature and σ_i is the respective standard deviation. With the normal transformation, all features have mean equal to 0 and standard deviation equal to 1 with respect to the training set.

Supervised Classification for Vessel Segmentation

The final segmentation was obtained by classifying the original input image pixels into two classes, namely vessel pixels and nonvessel pixels, according to the supervised classification approach.[18] A Bayesian classifier was adopted in which class likelihoods were described using Gaussian mixture models, providing a fast classification while still allowing complex decision surfaces. The class priors were estimated by the fraction of each class´ pixels present

in a training set composed of labelled samples, while the distribution parameters for each class´ Gaussian mixture model were estimated from the training set through the application of the Expectation-Maximisation algorithm.[32]

The training set was obtained from fundus images manually segmented by an ophthalmologist, providing labelled pixels as training samples. The training samples´ features were then normalised as described above and used to train the Bayesian classifier. The segmentation of new images was then generated by applying the classifier, without the need of tuning any additional parameters. The segmentation process can be implemented efficiently using the Fast Fourier Transform and the Fourier domain definition of the CWT for pixel feature generation[17], which takes time O(N log_2 N), where N is the total number of image pixels. The segmentation is obtained applying the Bayesian Gaussian mixture model classifier to all pixels, taking an additional O(N).

Some misclassified pixels appeared as undesirable noise in the output and as only boundaries were classified for some vessels, it was necessary to perform post-processing. The post-processing operations applied were 'area open' to eliminate small noisy components, 'dilation' and 'area close' to fill the vessels, followed by 'skeletonization' to extract the vessel branching pattern. The multiscale skeletonization algorithm based on exact dilations has been applied in this last step.[18] Morphological features were than extracted from the obtained vessel skeletons to distinguish such vessel patterns, as described in the next section.

Determination of morphological features

Automated classification into retinae with or without PDR requires high accuracy to be able to support screening programmes currently carried out by ophthalmologists. Seven morphological features associated with the skeletonised vessel pattern were determined: area, perimeter, circularity, curvature, orientation entropy, 2nd moment of the CWT and correlation dimension, with physical interpretations described as below. With the exception of the area, perimeter and

circularity, all are based on data obtained from the application of the derivatives-of-Gaussian wavelets to the automated segmented vessel skeletons.

Area

The area *A* estimation of the binary skeletons is obtained by simply counting the number of object pixels, taking linear time, Θ(N) in asymptotic notation, where N is the number of pixels in the image. It provides an approximation about the shape space occupation.

Perimeter

The perimeter *P* is obtained by counting the number of pixels of the vessel skeleton contour, also in linear time Θ(N).

Circularity

The circularity *C* is just the ratio between the shape square perimeter *P* and its area *A*, i.e. P^2/A. It shows how similar the shape is to a circumference and is rotation invariant, being often adopted as a shape complexity measure.[18] This calculation takes time Θ(1).

Wavelet transform for morphological analysis

Different differential morphological features were obtained, inspired by the shape analysis approach used for characterisation of retinal ganglion cells.[29] In this paper, we utilised the first derivative of the Gaussian function in order to compose a wavelet gradient. Therefore, we define two analysing wavelets $\psi_1(x,y)$ and $\psi_2(x,y)$ as partial derivatives of the Gaussian, ie. $\psi_1(x,y)=\frac{\partial g(x,y)}{\partial x}$ and $\psi_2(x,y)=\frac{\partial g(x,y)}{\partial y}$, where $g(x,y)$ denotes the 2D Gaussian.[20] By using $\psi_1(x,y)$ and $\psi_2(x,y)$ as wavelets, we can calculate the gradient wavelet as $\mathbf{T}_{\psi}[f](\mathbf{b},a)=\begin{pmatrix} T_{\psi_1}[f](\mathbf{b},a) \\ T_{\psi_2}[f](\mathbf{b},a) \end{pmatrix}$, where ψ, f, $\mathbf{b}$ and a denote respectively the analysing wavelet, analysed image, the displacement vector and scale factor. The wavelet transform

$\mathbf{T}_\psi[f](\mathbf{b},a)$ for each pair $(\mathbf{b},a)$ is actually a vector whose components are the respective coefficients of the wavelet transform using $\psi_1(x,y)$ and $\psi_2(x,y)$ as the analysing wavelets. Since the wavelet transform has been implemented so as to be calculated in the Fourier domain, the calculation of these numerical derivatives take time $\Theta(N\log_2 N)$. The morphological features described below are calculated based on the derivatives-of-Gaussian wavelet.

Curvature

The skeleton outline curvature represents how the direction of a unit tangent vector varies along the shape contour. It is described by:

$$k = \nabla . \frac{\nabla f}{\|\nabla f\|} = \frac{f_{xx} f_y^2 - 2 f_x f_y f_{xy} + f_{yy} f_x^2}{\left(f_x^2 + f_y^2\right)^{3/2}} \tag{1}$$

where f_x, f_y, f_{xx}, f_{yy} and f_{xy} denote the first partial derivatives of *f* with respect to *x* and to *y*, the second partial derivatives of *f* with respect to *x* and to *y*, and the partial derivative with respect to *x* and *y*, respectively.[33] These partial derivatives are estimated using the 2D wavelet transform in the same spirit described above for the gradients Thus given these partial derivatives, the curvature calculations take additional time $\Theta(N)$.

Orientation Entropy

The Orientation Entropy *E* indicates the orientation disorder degree encountered in a shape and is obtained from the angular distribution of the vector field defined by the wavelet gradient, as follows:

$$E = -\sum_{i \in K} p_i \ln(p_i) \tag{2}$$

where p_i is the occurrence frequency of some vector oriented towards the θ_i direction and K is the set of bins in the histogram. This calculation takes time proportional to the number of bins in the histogram, that is $\Theta(|K|)$.

CWT 2nd Moment

The 2nd Moment of the CWT modulus is a statistical dispersion measure to indicate biases in the gradient vector field. If q is the CWT Modulus histogram, with each bin q_i centered at i, then its CWT 2nd Moment is:

$$m_2^M = \sum_{i \in K} i^2 q_i \tag{3}$$

Similarly, this feature is calculated in time $\Theta(|K|)$.

Correlation Dimension

According to chaos theory, the correlation dimension (CD) measures the dimension of the space occupied by a set of random points, or put in another words it gives the probability of finding two points closer than a certain distance.[28, 34] This probability $C(\varepsilon)$ varies along with the considered distance ε which ranges between one pixel and the measure of the image diagonal. Usually, one might consider the mean, the median or the global $C(\varepsilon)$ value. Mathematically, CD is obtained by the correlation integral:

$$C(\varepsilon) = \lim_{N \to \infty} \frac{2}{N^2} \sum_{i=1, j>i}^{N} \theta\left(\varepsilon - \left| X_i - X_j \right|\right) \tag{4}$$

where the heaviside function is defined as:

$$\theta\left(\varepsilon - \left|X_i - X_j\right|\right) = \begin{cases} 1, if\left(\varepsilon - \left|X_i - X_j\right| \geq 0\right) \\ 0, if\left(\varepsilon - \left|X_i - X_j\right| < 0\right) \end{cases} \quad (5)$$

and the CD itself is taken as the slope of the logarithm of the correlation integral:

$$C(\varepsilon) \propto \varepsilon^{CD} \quad (6)$$

The CD curve itself is comprised of several short straight segments, among which the first and the last one should be disregarded, since in those regions the scales ε do not bring significant fractality information from the shape.[35]

To determine the upper and lower bound that is the singularities, we calculated the 3rd derivative. The 3rd derivative locates critical points found by the second derivative by searching for zero crossing points.[36] Hence, in order to find these region extremities, that is singularities, we calculated the 3rd derivative from C(ε), determining its zero crossing points, where those abrupt changes in slope take place. The 3rd derivative provides a vector of extremities for each segment of the curve. Thus by using the 3rd derivative information, we ignore the first and the last segments, sort the remaining ones and take the median value, resulting in the median CD value. The global CD value is obtained by disregarding the first slope segment and the last one and then considering the straight line between the points related to the second zero-crossing and the penultimate point in order to evaluate the global slope. The correlation integral (eq.4) takes time $\Theta(N^2)$, being the most time consuming feature calculation, while its derivatives calculations take an additional $\Theta(N\log_2 N)$.

Statistical analysis

Results for the features associated with automated and manual segmentation were compared using a two-sample t-test with unequal variance to test the hypothesis that the means were not significantly different. Linear discriminant analysis (LDA) was performed on the matrix

representing the data for each of the images (no retinopathy/background retinopathy versus neovascularisation present). Matrices were normalised so that each feature has zero mean and unit standard deviation followed by linear regression

A forward-backward feature selection process using LDA as the classifier was also applied to select the best features. This process can be shown to be a monotonically increasing function of the signal-to-noise ratio and using the area under the curve (AUC) indicates the effectiveness of the feature in discriminating between the two groups.

Results

The classifier output obtained from the original image is a binary image with labelled pixels as vessel or non-vessel. This binary image is post-processed and skeletonized, producing the results as illustrated in Figure 1.

Figure 1 Illustration of automated and manual skeletons compared to original grey scale image.

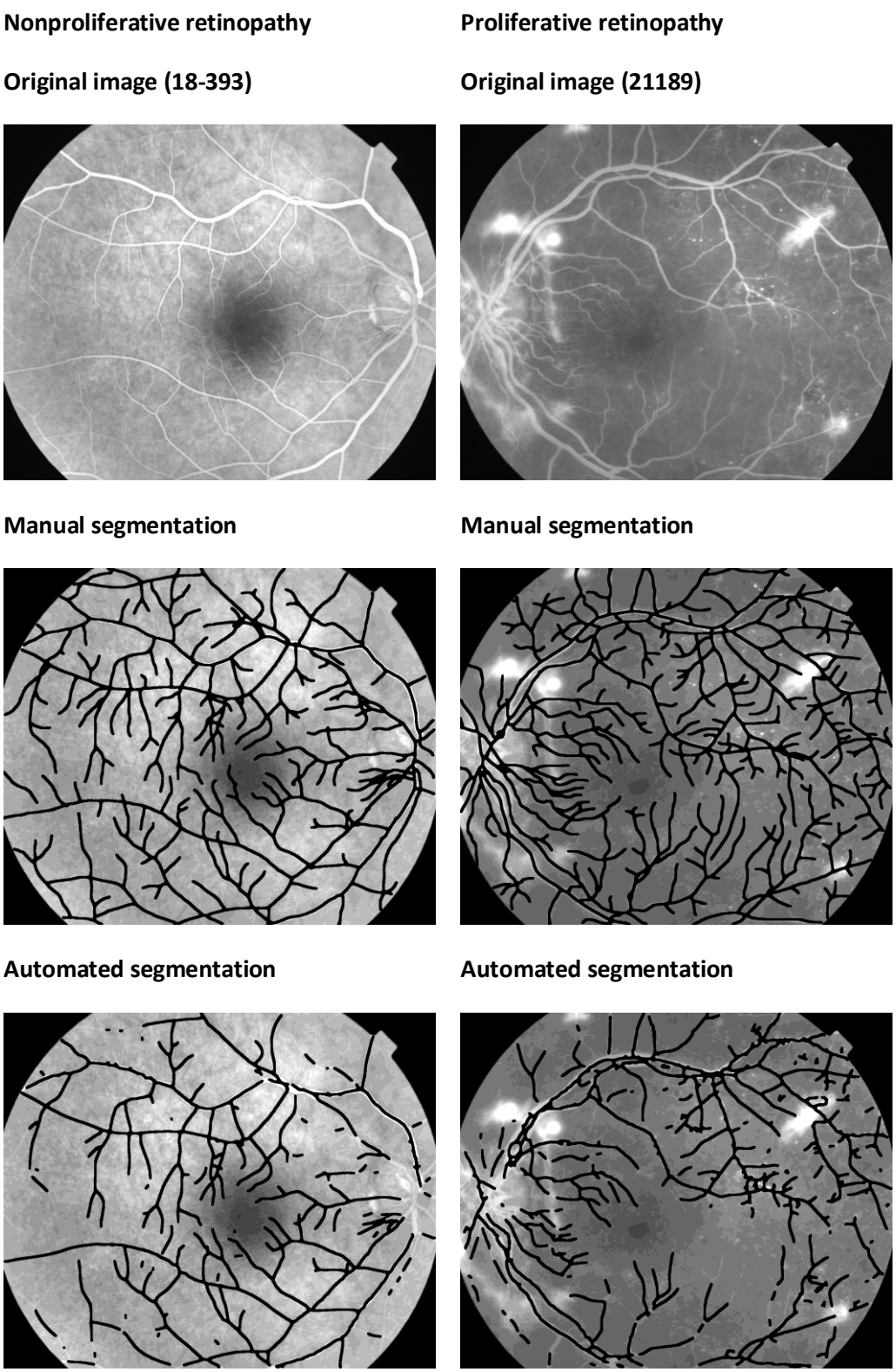

Illustration of outcome for automated and manual segmentation compared to original grey scale image. Overlaid skeletonized vessel pattern, in black, has been dilated for easier viewing. Note skeletons have been dilated for better viewing.

Figure 2 compares the outcome of the pattern analysis for orientation entropy and correlation integral for an image with and one without proliferative retinopathy.

Figure 2 Wavelet histograms for correlation integral and orientation entropy.

Nonproliferative retinopathy

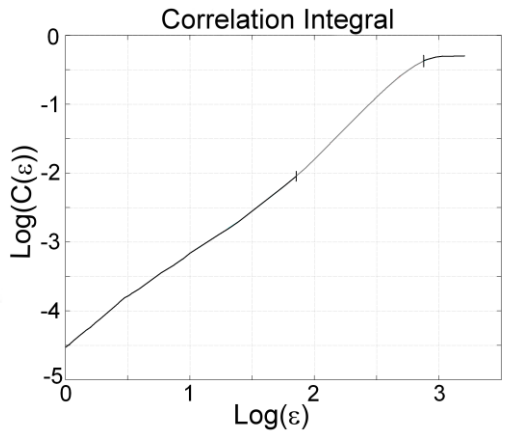

log-log of the correlation integral

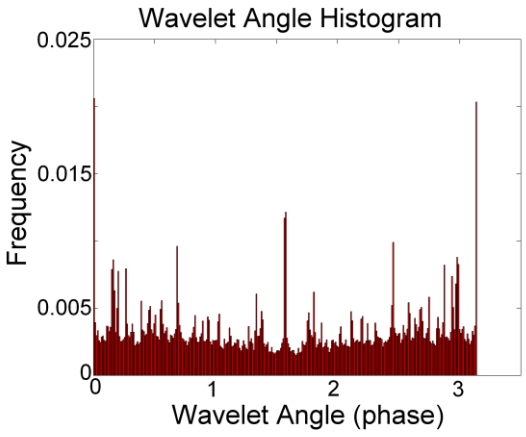

orientation entropy

Proliferative retinopathy

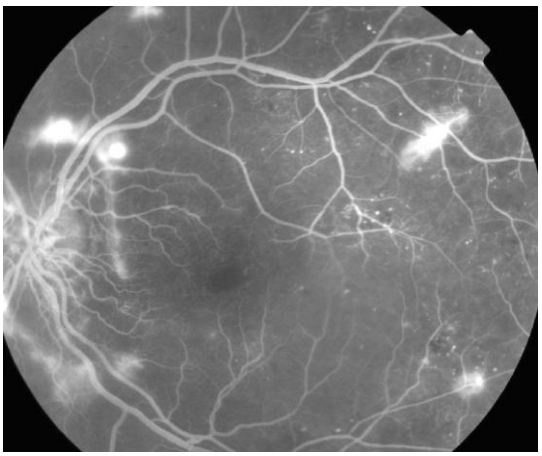

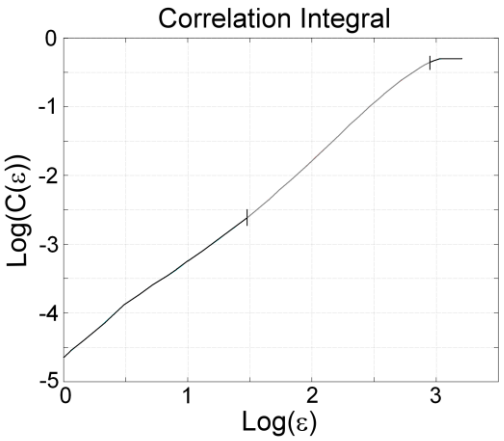

log-log of the correlation integral

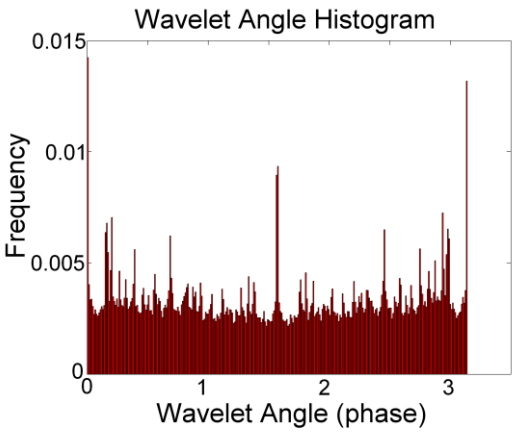

orientation entropy

Correlation integral and wavelet histogram for the orientation entropy comparing an image with neovascularisation to one with no neovascularisation. Vertical lines on the log-log correlation integral indicate upper and lower bound (see text).

Table 1 lists statistics of the seven features calculated between the manual and automated segmented images. Manual segmented images resulted in larger feature parameters except for circularity. A student t-test showed that the differences between the means of all features are statistically significant ($p < 0.001$), except for the entropy ($p = 0.38$). The differences arise because more vessels are identified by the observer than the automated procedure.

PUT TABLE 1 HERE

Since we are primarily interested in automated detection of PDR, we proceed to further analyse the automated data only. The data were normalized so that each feature has zero mean and standard deviation of one. The ability to use each feature individually to discriminate between non-PDR and PDR is summarized in Table 2. Only the curvature feature achieves statistical significance ($p = 0.042$) for a two-sampled t-test for the difference in means between the Non-PDR and PDR classes. However we are more interested in classification ability, and the area-under-curve (AUC) of the parametric bi-normal receiver operating characteristic (ROC) was also calculated.[37] The traditional features (area, perimeter and circularity) and the global CD are essentially random, thus have no classification ability (AUC = 0.49 in all cases). The wavelet based features (2nd moment, entropy, curvature and median CD) have some useful classification ability with AUCs of about 0.7. This indicates that these latter features are indeed more sensitive to the blood vessel branching patterns throughout the retina.

PUT TABLE 2 HERE

The above analysis considered features in isolation. A combination of features with an appropriate classifier may provide better predictive ability. We first tried forward-backward selection of features using the linear discriminant and Naïve-Bayes classifiers.[32] The AUC calculated from the resultant classifier was used as the criterion for selection or removal of features. We report AUCs with 95% confidence intervals (CI) as calculated by the ROCKIT program.[37] The best features identified using forward backward selection on the LDA classifier were median CD and wavelet 2nd moment with an AUC of 0.77 (0.56–0.91). Starting with all features and removing any that improved classification led to a set of six features (area, perimeter, entropy, curvature, median CD and global CD) with the LDA classifier achieving an AUC of 0.90 (0.73–0.97). As we are interested in the improvement provided by the wavelet based features we also ran LDA on the feature set comprising area, perimeter and circularity only, which achieved an AUC of 0.61 (0.37–0.82). Note that LDA based classification using traditional features (area, perimeter and circularity) fails statistical significance for better than random classification at the 95% confidence, whereas the wavelet based feature achieve statistically significant power to discriminate between PDR and non-PDR.

The Naïve-Bayes classifier shows similar results. Using just area, perimeter and circularity in a Naïve-Bayes classifier has an AUC of 0.58 (0.37–0.78) and fails statistical significance for better than random discriminatory power. Using the best four features (area, 2nd moment, entropy and global CD) identified by the forward-backward selection gives an AUC of 0.87 (0.67–0.96) which has statistically significant and useful discriminatory power. For the

Naïve-Bayes classifier, as with LDA, it is necessary to include some of the wavelet based features to discriminate between PDR and non-PDR.

Figure 3 Receiver operating characteristics (ROC) curve.

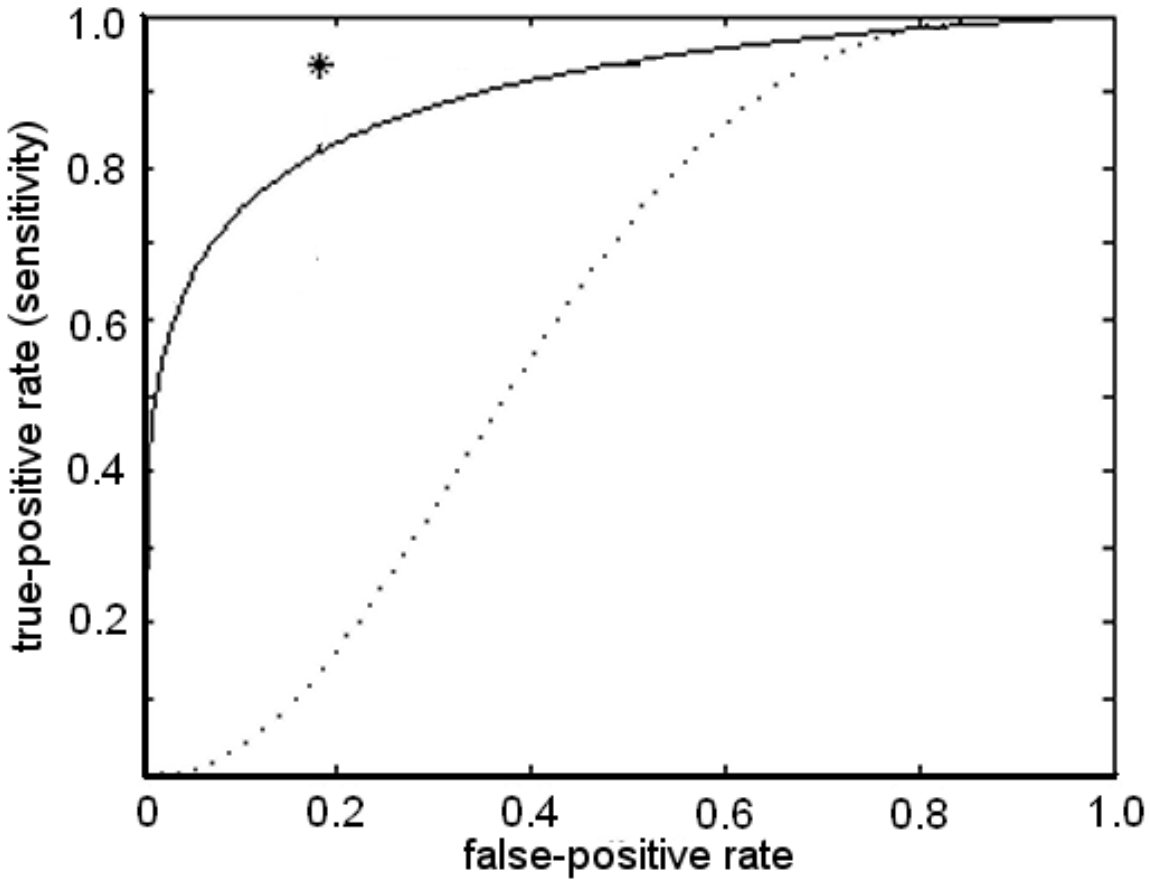

Receiver operating characteristics (ROC) curve for automated segmented images using the six best feature set. * indicates operating point; solid line: six best features; short dash line: traditional features (area, perimeter, circularity).

We show in figure 3 the full ROC curve (fitted to the data with the parametric bi-normal model due to Metz) for the LDA classifier operating on the best six features identified above and the ROC curve fitted to the LDA classifier operating on the traditional three features.

Using the 'best six features' and the LDA classifier at the operating point marked with an asterisk on the ROC curve, figure 3, three images were incorrectly classified. Of these, one was opaque and bad quality, whilst the second had a venous loop present. The third was of good quality with neovascularisation present both near the disc and in the periphery. Thus the classifier achieved 15 true-positives out of 16 images (sensitivity of 94%) and 2 false-positives out of 11 negatives (false-positive rate of 18%) giving a specificity of 82% using automatically segmented images.

Discussion

The importance of our work lies in combining automated segmentation procedures with automated recognition of proliferative retinopathy using features determined from the wavelet derived results such as the 2nd wavelet moment, entropy and the median correlation dimension. In addition we have aimed at using a clinical relevant sample that included images where the quality was not optimal and those with panretinal laser surgery scars, diverse progression of retinopathy and proliferation either showing as areas of ischaemia, or new blood vessels near the optic disc or in the periphery. The results obtained were produced using the same configuration parameters for all images, pre-processing and optic disc removal to improve the vessel segmentation was also not required due to the nature of the wavelet transform. This is a major step forward in automated segmentation and analysis as it decreases the computation time and operator involvement.[10] Nevertheless differences between the manual and automated segmentation can be noted (Figure 1). Quality of image either associated with methodology or pathology not only influences automated methods but also manual segmentation as can be seen in the STARE database (http://www.parl.clemson.edu/stare/). These errors are however randomly distributed across

the nonproliferative and proliferative retinopathy images and should not have influenced the outcome of our classification.

Previous work comparing the CWT to other segmentation methods using the STARE and DRIVE database images as the golden standard showed that supervised learning and adaptive thresholding obtained a greater than 75% sensitivity for vessel segmentation.[15]. A comparison of six segmentation methods including our CWT indicated a similar outcome with the sensitivity and specificity being greater then 80%.[16]

Ophthalmologists have an 80 to 95% success rate in identifying proliferative retinopathy. This success rate decreases with eye media opacification and for identifying earlier stages of proliferation. However non-specialists perform no better than chance (50%).[38] Traditional features such as area or perimeter are not sensitive enough to discriminate between the non-proliferative retinopathy and retinal fundi displaying neovascularisation. This is because area and perimeter only pick up the total amount of vasculature, whereas PDR involves a reconfiguration of the vasculature. It is necessary therefore to use features that are sensitive to the branching and space filling nature of the vessel pattern, such as the wavelet based features that we employed.

Our feature analysis suggests that utilising the six best features that include median correlation dimension, curvature and entropy provides the most accurate classification with 94% sensitivity and 82% specificity. The three images classified incorrectly included one with opacity, whilst another had advanced nonproliferative retinopathy and the third had a venous loop and Hollenhorst plaques in addition to diabetic retinopathy present. As such, including additional image analysis tools such as an microaneurysm detector may improve these findings. The use of digital non-mydriatic colour images for routine community screening has been shown to be effective but will lead to a further challenge for detecting

early stage proliferative retinopathy using automated methods. In addition, other classifiers than the LDA or Naïve-Bayes reported here may also improve the classification results and this is being investigated currently on a larger set of images.

One of the advantages of our morphological feature set is that it identified images that contain neovascularisation within the retina but not present in the view of the posterior pole suggesting that peripheral changes associated with neovascularisation leads to a remodelling throughout the retina.

Acknowledgements

HJ was in receipt of a Charles Sturt University grant (A514 713 9661). RMC and JVBS are grateful to FAPESP (2005/00587-5 and 2006/56128-1) and to CNPq (300722 /98-2, 474596/2004-4, 131403/2004-4 and 491323/2005-0). We like to thank Cherryl Kolbe and Bev deJong for technical assistance. Chris McQuellin was responsible for the retinal photography.

References

1. H. R. Taylor and J. E. Keeffe, "World blindness: a 21st century perspective," Br. J. Ophthalmol. **85**, 261-266 (2001).
2. K. Viswanath and M. McGavin, "Diabetic retinopathy: clinical findings and management," Community Eye Health **16**(4), 21-24 (2003).

3. K. S. Coyne, M. K. Margolis, T. Kennedy-Martin, T. M. Baker, R. Klein, M. D. Paul, and D. A. Revicki, "The impact of diabetic retinopathy: perspectives from patient focus groups," Fam. Pract. **21**(4), 447-453 (2004).

4. J. Kanski, *Clinical Ophthalmology: A systematic approach* (Butterworth-Heinemann, London, 1989), pp. 465-479.

5. U. Freudentsin and J. Verne, "A national screening programme for diabetic retinopathy," BMJ **323**, 4-5 (2001).

6. S. J. Lee, C. Sicari, C. A. Harper, H. R. Taylor, and J. E. Keeffe, "Program for the early detection of diabetic retinopathy: A two-year follow-up.," Clin. Exp. Ophthalmol. **29**, 12-25 (2001).

7. T. Walter, J. C. Klein, P. Massin, and F. Zana, "Automated segmentation and registration of retinal fluorescein angiographies," presented at the Proc. International Workshop on Computer Assisted Fundus Image Analysis, Herlev Hospital, Copenhagen, Denmark, 2000.

8. X. W. Gao, A. Bharath, A. Stanton, A. Hughes, N. Chapman, and S. Thom, "Quantification and characterisation of arteries in retinal images," Comp. Meth. Prog. Biomed. **63**(2), 133-146 (2000).

9. A. Hoover, V. Kouznetsova, and M. Goldbaum, "Locating blood vessels in retinal images by piecewise threshold probing of a matched filter response," Medical Imaging **19**(3), 203-210 (2000).

10. F. Zana and J.-C. Klein, "Segmentation of vessel-like patterns using mathematical morphology and curvature evaluation," IEEE Transactions on Image Processing **10**(7), 1010-1019 (2000).

11. C. Kirbas and F. Quek, "A review of vessel extraction techniques and algorithms," ACM Comput. Surv. **32**(2), 81-121 (2004).

12. X. Jiang and D. Mojon, "Adaptive local thresholding by verification-based multithreshold Probing with application to vessel detection in retinal images," IEEE Transactions on Pattern Analysis and Machine Intelligence **25**(1), 131-137 (2003).

13. J. J. Staal, M. D. Abràmoff, M. Niemeijer, M. A. Viergever, and B. van Ginneken, "Ridge based vessel segmentation in color images of the retina," IEEE Transactions on Medical Imaging **23**(4), 501-509 (2004).

14. D. Nain, A. Yezzi, and G. Turk, "Vessel Segmentation Using a Shape Driven Flow," presented at the Medical Image Computing and Computer-assisted Intervention - MICCAI, 2004.

15. D. Cornforth, H. F. Jelinek, J. J. G. Leandro, J. V. B. Soares, J. Cesar, R.M., M. J. Cree, P. Mitchell, and T. Bossomaier, "Evolution of retinal blood vessel segmentation using wavelet transform in assessment of diabetic retinopathy," Complexity International **11**, http://www.complexity.org.au/ci/vol11/ (2005).

16. M. J. Cree, J. J. G. Leandro, J. V. B. Soares, J. Cesar, R.M. , H. F. Jelinek, and D. Cornforth, "Comparison of various methods to delineate blood vessels in retinal images," presented at the Proceedings of the 16th Australian Institute of Physics Congress, 2005.

17. J. V. B. Soares, J. J. G. Leandro, R. M. Cesar-Jr, H. F. Jelinek, and M. J. Cree, "Vessel segmentation using the 2-D Gabor wavelet and supervised classification," IEEE Transactions in Medical Imaging **25**(9), 1214-1222 (2006).

18. L. F. Costa and R. M. Cesar Jr, *Shape Analysis and Classification: Theory and Practice* (CRC Press, 2001).

19. J. P. Antoine, D. Barache, R. M. CesarJr., and L. F. Costa, "Shape characterization with the wavelet transform," Signal Processing **62**(3), 265-290 (1997).

20. A. Arnéodo, N. Decoster, and S. G. Roux, "A wavelet-based method for multifractal image analysis. I. Methodology and test applications on isotropic and anisotropic random rough surfaces," Eur. Phys. Journal B **15**, 567-600 (2000).

21. A. Grossmann, "Wavelet Transforms and Edge Detection," in *Stochastic Processes in Physics and Engineering*, S. Albeverio, P. Blanchard, M. Hazewinkel, and L. Streit, eds. (Reidel Publishing Company, 1988).

22. M. J. Cree, J. A. Olson, K. McHardy, P. Sharp, and J. Forrester, "A fully automated comparative microaneurysm digital detection system.," Eye **11**, 622-628 (1997).

23. J. Hipwell, F. Strachan, J. Olson, K. McHardy, P. , Sharp, and J. Forrester, "Automated detection of microaneurysms in digital red-free photographs: a diabetic retinopathy screening tool.," Diabetic Medicine **17**, 588-594. (2000).

24. C. Sinthanayothin, J. F. Boyce, H. Cook, and T. Williamson, "Automated localisation of the optic disc, fovea and retinal blood vessels from digital colour fundus images.," Br. J. Ophthalmol. **83**(8), 902-912. (1999).

25. A. Osareh, M. Mirmehdi, B. Thomas, and R. Markham, "Automated identification of diabetic retinal exudates in digital colour images," Br. J. Ophthalmol. **87**, 1220-1223 (2003).

26. M. E. Martinez-Perez, A. D. Hughes, A. V. Stanton, S. A. Thom, N. Chapman, A. A. Bharath, and K. H. Parker, " Retinal vascular tree morphology: A semi-automatic quantification," IEEE Transactions on Biomedical Engineering **49**(8), 912-917 (2002).

27. J. Cesar, R. M. and H. F. Jelinek "Segmentation of retinal fundus vasculature in nonmydriatic camera images using wavelets," in *Angiography and plaque imaging*, J. S. Suri and S. Laxminarayan, eds. (CRC Press, 2003), pp. 193-224.

28. B. R. Masters, "Fractal analysis of the vascular tree in the human retina," Annual Rev. Biomed. Eng. **6**, 427-452 (2004).

29. H. F. Jelinek, R. M. Cesar, Jr., and J. J. G. Leandro, "Exploring wavelet transforms for morphological differentiation between functionally different cat retinal ganglion cells," Brain and Mind **4**, 67-90 (2003).

30. J. P. Antoine, P. Carette, R. Murenzi, and B. Piette, "Image analysis with two-dimensional wavelet transform," Signal Processing **31**, 241-272 (1993).

31. J. J. G. Leandro, J. V. B. Soares, J. Cesar, R.M., and H. F. Jelinek, "Blood vessel segmentation of non-mydriatic images using wavelets and statistical classifiers," presented at the Proceedings of the Brazilian Conference on Computer Graphics, Image Processing and Vision (Sibgrapi), pp. 262-269 (2003).

32. R. O. Duda, P. E. Hart, and D. G. Stork, *Pattern classification,* 2 ed. (Wiley Interscience, 2001).

33. L. F. Estrozi, L. G. Rios, A. G. Campos, R. M. Cesar-Jr., and L. d. F. Costa, "1D And 2D Fourier-based approaches to numeric curvature estimation and their comparative performance assessment.," Digital Signal Processing **13**, 172-197 (2003).

34. P. Asvestas, G. K. Matsopoulos, and K. S. Nikita, "Estimating of fractal dimension of images using fixed mass approach," Pattern Recognition Letters **20**, 347-354 (1999).

35. J. P. Rigaut, "An empirical formulation relating boundary lengths to resolution in specimens showing 'non-ideally fractal' dimensions.," J. Microsc. **133**, 41-54 (1984).

36. R. C. Gonzalez, R. E. Woods, and S. L. Eddins, *Digital image processing using Matlab* (Pearson Prentice Hall, 2004).

37. C. E. Metz, "ROC methodology in radiologic imaging," Investigative Radiol. **21**, 720-733 (1986).

38. E. Sussman, W. Tsiaras, and K. Soper, "Diagnosis of diabetic eye disease," JAMA **247**, 3231-3234 (1982).

Table 1. Feature comparison for manual and automated segmented images.

Feature	Manual Segmentation (Mean±sd)*	Automated Segmentation (Mean±sd)	t-statistic	p-value
Area	102000±23000	24600±5200	-17.0	< 0.0001
Perimeter	31200±5200	24400±8400	-6.74	< 0.0001
Circularity	13500±3000	24300±5100	9.38	< 0.0001
2nd Moment	4362±25	1080±24	-493	< 0.0001
Entropy	5.63±0.01	5.62±0.02	-0.9	0.38**
Curvature	178.0±3.9	133.6±4.3	-39.9	< 0.0001
Median CD***	1.67±0.1	1.42±0.1	-11.8	< 0.0001
Global CD	1.58±0.04	1.49±0.04	-8.2	< 0.0001

* Mean ± standard deviation; ** non significant; *** correlation dimension

Table 2. Comparison between nonproliferative and proliferative diabetic retinopathy for the eight features analysed.

Feature	Non PDR	PDR	t statistic	p value	AUC*
Area	0.038±0.82	-0.026±1.1	0.169	0.87	0.49
Perimeter	0.040±0.82	-0.027±1.1	0.178	0.86	0.49
Circularity	0.041±0.82	-0.029±1.1	0.186	0.85	0.49
2^{nd} moment	-0.35±0.63	0.24±1.1	-1.74	0.095	0.72
Entropy	-0.41±1.3	0.28±0.65	-1.64	0.12	0.70
Curvature	-0.46±0.85	0.31±1.0	-2.15	0.042	0.76
Median CD**	-0.44±1.1	0.30±0.87	-1.93	0.068	0.70
Global CD	-0.065±0.82	0.45±1.1	-0.292	0.77	0.49

* area under curve; ** correlation dimension

REFERENCES